AD NUMBER

AD801326

LIMITATION CHANGES

TO:

Approved for public release; distribution is unlimited.

FROM:

Distribution authorized to U.S. Gov't. agencies and their contractors; Critical Technology; JUN 1966. Other requests shall be referred to Air Force Systems Command Space Sytems Division, Los Angeles AFB, CA 90009-2960. This document contains export-controlled technical data.

AUTHORITY

SAMSO ltr, 24 Jan 1972

AIR FORCE REPORT NO.
SSD-TR-66-175

AEROSPACE REPORT NO.
TR-669(6230-25)-4

Optical Absorption and Fluorescence Intensities in Several Rare-Earth-Doped Y_2O_3 and LaF_3 Single Crystals

JUNE 1966

Prepared by WILLIAM F. KRUPKE
Electronics Research Laboratory
Laboratories Division
Laboratory Operations
AEROSPACE CORPORATION

Prepared for BALLISTIC SYSTEMS AND SPACE SYSTEMS DIVISIONS
AIR FORCE SYSTEMS COMMAND
LOS ANGELES AIR FORCE STATION
Los Angeles, California

NOTICE

This document is subject to special export controls and each transmittal to foreign governments or foreign nationals may be made only with prior approval of SSD (SSTRT).

Air Force Report No.
SSD-TR-66-175

Aerospace Report No.
TR-669(6230-25)-4

OPTICAL ABSORPTION AND FLUORESCENCE INTENSITIES IN SEVERAL RARE-EARTH-DOPED Y_2O_3 AND LaF_3 SINGLE CRYSTALS

Prepared by

William P. Krupke
Electronics Research Laboratory

Laboratories Division
Laboratory Operations
AEROSPACE CORPORATION

June 1966

Prepared for

BALLISTIC SYSTEMS AND SPACE SYSTEMS DIVISIONS
AIR FORCE SYSTEMS COMMAND
LOS ANGELES AIR FORCE STATION
Los Angeles, California

FOREWORD

This report is published by the Aerospace Corporation, El Segundo, California, under Air Force Contract No. AF 04(695)-669.

This report, which documents research carried out from 1 July 1965 through May 1966, was submitted 14 September 1966 to Captain Ronald J. Starbuck, SSTRT, for review and approval.

The author appreciatively acknowledges stimulating discussions with Dr. Isaac Richman and Dr. John Gruber concerning the theoretical aspects of the crystal-field-induced transition model, and with Dr. N. C. Chang concerning the properties of the Y_2O_3 lattice. Without the numerous crystal samples kindly provided by Armond Chase and Miss Judy Osmer, this study would not have been possible.

Approved

D. D. King, Director
Electronics Research Laboratory
Laboratories Division
Laboratory Operations

Publication of this report does not constitute Air Force approval of the report's findings or conclusions. It is published only for the exchange and stimulation of ideas.

Ronald J. Starbuck, Captain
Space Systems Division
Air Force Systems Command

ABSTRACT

The absolute intensities of transitions occurring in the optical spectra of single crystals of Y_2O_3 doped with small amounts of Pr, Nd, Eu, Er, and Tm; single crystals of LaF_3 doped with small amounts of Pr and Nd; and single crystals of Er_2O_3, Tm_2O_3, and Yb_2O_3 have been measured at room temperature. All observed transitions occur within the ground configurations of the trivalent rare-earth ions, and their intensities are accounted for using three phenomenological parameters for each system, whose values are determined by a least-squares fitting calculation. A calculation of the relevant crystal-field terms is made, and theoretical values for the intensity parameters are calculated using free-ion radial wave functions and certain closure approximations. It is concluded that excited $4f^{n-1}g$ configurations contribute to observed intensities more than is indicated by free-ion calculations, and that the excited $4f^{n-1}5d$ configuration contributes to the observed intensities an order of magnitude less than indicated by free-ion calculations. A hypersensitive transition in the neodymium systems is observed and its sensitivity is traced to a simple change in point symmetry of the host.

CONTENTS

FOREWORD ii

ABSTRACT iii

I. INTRODUCTION 1

II. THEORETICAL CONSIDERATIONS 3

III. EXPERIMENTAL DETAILS 7

IV. EXPERIMENTAL AND CALCULATED INTENSITIES 11

V. VALIDITY OF THE MODEL 15

VI. INTERPRETATION OF EXPERIMENTAL PARAMETERS 17

VII. TRANSITION INTENSITIES IN RE:LaF_3 31

VIII. CONCLUSIONS 35

APPENDIX 37

REFERENCES 43

FIGURES

1. Experimental intensity parameters ($\bar{\Omega}_\lambda$) and theoretical static intensity parameters (Ω_λ), based on free-ion radial wave functions as a function of the number of 4f electrons 18

2. Scale diagram of the C_2 cation site of Y_2O_3 showing the six nearest-neighbor oxygen ions 19

TABLES

I. Measured and calculated f numbers for $Pr^{3+}:Y_2O_3$ 11

II. Measured and calculated f numbers for $Pr^{3+}:LaF_3$ 11

III. Measured and calculated f numbers for $Nd^{3+}:Y_2O_3$ 12

IV. Measured and calculated f numbers for $Nd^{3+}:LaF_3$ 12

V. Measured and calculated transition probabilities for $Eu^{3+}:Y_2O_3$ 12

VI. Measured and calculated f numbers for $Er^{3+}:Y_2O_3$ 12

VII. Measured and calculated f numbers for Tm_2O_3 13

VIII. Experimental intensity parameters, $\bar{\Omega}_\lambda$ 13

IX. Odd-degree lattice sums for Y_2O_3, C_2 site 20

X. Radial moments between 4f and excited electronic configurations, and energy denominators 22

XI. Calculation of free-ion $\Xi(t, \lambda)$ 24

XII. Theoretical intensity parameters using free-ion radial wave functions 24

XIII. Racah and spin-orbit parameters used to generate intermediate coupling wave functions 38

I. INTRODUCTION

Intensities of transitions observed in the spectra of rare-earth-doped solutions and solids have come under quantitative study within the last few years. Judd[1] and Ofelt[2] independently have discussed a general theoretical framework for calculating the intensities of such transitions, and have carried out the complex Racah algebra that yields expressions for transition strengths which lend themselves to correlation with experimental intensity data. The good agreement found by Judd, between calculated and measured oscillator strengths for solutions containing rare-earth ions, prompted Axe[3] to test the theory in more detail by examining the fluorescence intensities of the observed electric and magnetic dipole transitions between individual Stark components of Eu^{3+} ions in europium-ethylsulfate single crystals. Somewhat later, Krupke and Gruber[4] studied the optical absorption intensities of inter-Stark transitions observed in the spectrum of thulium ethylsulfate single crystals. Both studies confirmed that the proposed theory of crystal-field-induced electric dipole transitions between individual Stark components could account for observed intensities with reasonable accuracy using only a few phenomenological parameters.

Attempts to calculate the experimentally determined parameters using free-ion radial wave functions has met with little success, and it is in this area that the present work is directed. To establish the source of the difficulty in interpreting the experimental parameters, two types of studies come to mind: (1) studying the spectral intensities of a specified rare-earth ion in a number of different hosts, and (2) studying the spectral intensities of a number of different rare-earth ions in a common host. In (1), the radial properties of the rare-earth ion remain unaltered, and the lattice field changes from system to system. In (2), the lattice field remains unaltered, while the radial properties of each system are different. During the preparation of this manuscript Carnall, et al.,[5] reported the results of a study addressed primarily to (1). The spectral intensities of rare-earth solutions were observed and accounted for phenomenologically. The lack of

knowledge of the local charge distribution precluded a calculation of the experimentally determined parameters, and thus could not shed light on the problem of radial wave functions. This report presents the results of a study addressed primarily to (2).

Spectral intensities were measured for single crystals of Y_2O_3 doped with small amounts of praeseodymium, neodymium, europium, erbium, thulium, single crystals of LaF_3 doped with praeseodynium and neodymium, and single crystals of erbium, thulium, and ytterbium oxide. These systems span the rare-earth series and provide a wide variation in the radial properties of the excited electronic configurations. The lattice parameters of Y_2O_3 are sufficiently well known to permit a calculation of the pertinent odd-degree crystal-field lattice sums. With these values known, the contribution of various excited configurations can be studied.

II. THEORETICAL CONSIDERATIONS

The integrated absorption coefficient, $\int k(\lambda)d\lambda$, due to an electric dipole transition within the $4f^n$ electronic configuration of a rare-earth ion in a crystalline lattice, may be written[6]

$$\int k(\lambda)d\lambda = \rho \frac{8\pi^3\bar{\lambda}}{3ch}\left[\frac{(n^2+2)^2}{9n}\right] \left|\sum_{i,j} \langle i|P|j\rangle\right|^2 , \qquad (1)$$

where ρ is the rare-earth-ion density in the lattice and $n = n(\bar{\lambda})$ is the index of refraction of the bulk isotropic dielectric medium at the mean wavelength of the transition $\bar{\lambda}$. P is the electric dipole moment operator, $P = -e\Sigma r_i$ for a transition between the initial and final states. In the free-ion approximation, the states of the $4f^n$ configuration are taken as a linear combination of Russell-Saunders states $|4f^n, S, L\rangle$:

$$|4f^n[S,L]J\rangle = \sum_{S,L} A(S,L,J)|4f^n S,L\rangle . \qquad (2)$$

In these "intermediate-coupling" wave functions, the quantum numbers S and L, which are convenient labels for states, but which are not good quantum numbers, are enclosed in brackets. The matrix of P between states of the form (2) is identically zero, since the Russell-Saunders states, and hence initial and final states, have the same parity. To obtain a nonzero electric dipole matrix element, wave functions of states of opposite parity must be mixed into the wave functions associated with at least one of the two J levels involved in the transition. When the rare-earth ion is in a crystal site without inversion symmetry, the most important mechanism for mixing in opposite parity wave functions is due to the odd-parity terms of the static crystalline

Stark field. The electric field also removes, at least partially, the (2J + 1)-fold degeneracy of the free-ion J levels, giving rise to the familiar crystal-field Stark splitting. A generally weaker mechanism which can also contribute to the electric dipole matrix is the interaction of lattice phonons of suitable symmetry with the electronic states.[7] This interaction is usually dominant in producing the spectra of rare-earth ions placed in crystal sites with inversion symmetry, since the contribution from the static crystalline field is then zero.

Based on the analysis of Judd[1] the total integrated absorption coefficient for electric-dipole transitions between initial level J and terminal level J' may be written

$$\int k(\lambda)d\lambda = \rho \frac{8\pi^3 e^2}{3ch(2J+1)} \left[\frac{(n^2+2)^2}{9n}\right] \sum_{\lambda=2,4,6} (\Omega_\lambda + \Omega_\lambda') \times |\langle 4f^n[S,L]J||U^{(\lambda)}||4f^n[S',L']J'\rangle|^2 \quad . \tag{3}$$

Similarly, the total transition probability, $A([S,L]J;\ [S',L']J')$ for electric dipole transitions between excited level J and the lower lying terminal level J', due to spontaneous emission, is

$$A([S,L]J;[S'L']J') = \frac{64\pi^4 e^2}{3h(2J+1)\bar{\lambda}^3} \left[\frac{n(n^2+2)^2}{9}\right] \sum_{\lambda=2,4,6} (\Omega_\lambda + \Omega_\lambda') \times |\langle 4f^n[SL]J||U^{(\lambda)}||4f^n[S',L']J'\rangle|^2 \quad . \tag{4}$$

Expressions (3) and (4) are valid provided the energy splitting of the initial J level is less than kT, where T is the crystal temperature at which the spectral intensities are measured. This requirement arises from the principle of spectroscopic stability which states that the total transition strength between

two levels which are each degenerate is unaltered under a perturbation splitting of the levels if the split components of the initial level are equally occupied. The matrix elements $U^{(\lambda)}$ are the doubly reduced matrix elements of the spherical tensor operators, calculated in the intermediate coupling approximation. The Russell-Saunders values of the $U^{(\lambda)}$ are readily calculated using the tabulations of Nielson and Koster[8] and of Rotenbert, et al.[9] The transformation from Russell-Saunders coupling to intermediate coupling is then made using the wave functions, Eq. (2). The two terms, $\Omega_\chi, \Omega_\lambda'$, arising, respectively, from the static crystal field and the vibronic-electronic interaction involving single phonons, are given by[1]

$$\Omega_\lambda = (2\lambda + 1) \sum_{t,p} |A_{tp}|^2 (2t + 1)^{-1} \Xi^2(t, \lambda) \tag{5}$$

and

$$\Omega_\lambda' = (2\lambda + 1) \sum_{t,p,\eta,\eta'} (2t + 1)^{-1} |\langle \eta | Q_i | \eta' \rangle|^2 \times \rho(\eta) \left| \frac{\partial A_{tp}}{\partial Q_i} \right|^2 \Xi^2(t, \lambda) \quad . \tag{6}$$

In Eq. (5), the $A_{tp}(t, \text{odd})$ are the odd-parity terms in the static crystal field expansion; in Eq. (6), Q_i denotes the normal coordinate of the vibrating complex, η, η' denote the totality of vibrational quantum numbers of the initial and final vibrational states, and $\rho(\eta)$ is the density of states. The quantities $\Xi(t, \lambda)$ contain integrals involving the radial parts of the $4f^n$ wave functions and the excited opposite-parity electronic-state wave functions, and the energies separating these states.

Magnetic dipole transitions are allowed between states of the same parity and can be of sufficient strength in certain cases to contribute to the observed intensities. In the limit of LS coupling, transitions from the ground state to the first excited state of the ground multiplet will be the only

allowed magnetic-dipole transitions. Inclusion of the spin-orbit interaction may permit a few additional transitions between ground state and other excited J levels. The evaluation of the magnetic-dipole transition intensities is straightforward.[10,11] The calculated intensities of the significant magnetic dipole transitions in the systems studied agree exactly with those found by Axe[3] and by Carnall, et al.,[5] and will not be reproduced here. In cases where magnetic-dipole transitions are significant, the calculated value of the magnetic-dipole intensity was subtracted from the total measured intensity; and the remainder was assigned to an electric-dipole transition.

To interpret the experimental data, the following fitting procedure was used. The numerical values of the three parameters Ω_λ, appearing in the sum

$$S = e^2 \sum_{\lambda=2,4,6} \Omega_\lambda \left| 4f^n[S, L]J \right| \left| U^{(\lambda)} \right| \left| 4f^n[S', L']J' \right\rangle \Big|^2 \qquad (7)$$

were varied in such a way as to minimize the sum of the squares of the deviations between measured and calculated values of S, the transition-line strength. For convenience in presenting the data and the results of the fitting, intensities are reported in terms of the oscillator strength or f number, which is a dimensionless quantity and is simply related to the line strength by[11]

$$f = \frac{8\pi^2 mc}{3h\bar{\lambda}(2J+1)e^2} \left[\frac{(n^2+2)^2}{9n} \right] S \qquad . \qquad (8)$$

The quantity of the fitting can be expressed by the smallness of the root mean square (rms) deviation in f number, defined by

$$\text{rms dev.} = \left[\frac{(\text{sum of squares of dev. in f numbers})}{(\text{no. of levels fit}) - (\text{no. of parameters})} \right]^{1/2} \qquad (9)$$

III. EXPERIMENTAL DETAILS

Single-crystal samples of Y_2O_3 doped with nominally 1% and 5% Nd, Eu, Er, and Tm and pure Er_2O_3, Tm_2O_3, and Yb_2O_3 single crystals, all measuring approximately 3 mm × 3 mm × 10 mm, were grown by the flame-fusion method.[12] The samples were polished with flat and parallel faces, with thicknesses varying between 0.05 and 0.25 cm, each thickness being chosen to result in a suitable display of absorption intensities for that sample. Single crystals of nominally 1% Pr^{3+}: LaF_3, 5% Nd^{3+}: LaF_3 and pure PrF_3 and NdF_3 were purchased commercially and mechanically prepared in the same manner as the Y_2O_3 samples.

The absorption spectra of these samples were recorded using a Cary Model 14 spectrophotometer in the spectral region from 2000 Å to 2.5 μ. The crystals were at room temperature, and at this temperature the observed spectral linewidths were always considerably larger than the instrumental resolution. The crystals were mounted on a baffle in order that all light reaching the detector would pass through the sample. The Cary spectrophotometer provides a graph of the spectral absorption coefficient, $k(\lambda)$, as a function of the wavelength, λ. The chart speed and scanning rate were in each case selected so that the pen writing speed was well below the maximum allowed and the resulting areas were always greater than 10 cm^2. The areas under the experimental spectral curves were measured with a K & E 620015 compensating polar planimeter.

Fluorescence of various samples was excited using a suitably filtered 1-kW, AH6 mercury arc lamp, and measured using a half-meter Jarrell-Ash monochromator with a dispersion of 16A/mm and a slit width equivalent to 0.5 Å throughout the spectral region studied, 4000 to 8200 Å. A single detector, an RCA 7265 photomultiplier, was used in order to obtain a precise measure of the relative fluorescence intensities. The spectral response of the entire measuring system including detector, grating, and optical system,

was determined using a standard filament tungsten lamp calibrated by the National Bureau of Standards. Measured fluorescence intensities were corrected for system spectral response.

A General Radio Strobotac Xenon flash lamp producing a pulse of about 5 μsec duration, was used to excite fluorescence in the sample crystals to determine fluorescence lifetime. The fluorescence radiation was passed through the monochromator, and its intensity as a function of time was displayed on an oscilloscope.

The relatively large value of index of refraction of Y_2O_3 and its large dispersion over the spectral region studied makes the index of refraction term in Eq. (3) important. The indices of refraction have been measured[13] to be 1.915 and 1.962 for Y_2O_3 and Er_2O_3, respectively, at a wavelength of 5690 Å; indices for these materials at other wavelengths have not been reported. In the absence of more precise data, it has been assumed that the dispersion of the index of refraction is reasonably accounted for by the simple Cauchy equation, $n(\lambda) = a + b/\lambda^2$. To evaluate the constants a and b, a second value of the index of refraction of Y_2O_3 was required. The reflection-coefficient of Y_2O_3 was measured at 2600 Å and used to calculate the index of refraction at the same wavelength. This value and the value of n at 5690 Å were used to determine the Cauchy constants a = 1.780 and b = 0.0598 μ^2 for Y_2O_3. The index of refraction of single crystal LaF_3 has been measured at a number of wavelengths between 0.4 and 2.2 μ,[14] and simple interpolation provides the indices at other wavelengths. Over the spectral region studied, the dispersion is only 5% for LaF_3, but about 100% for Y_2O_3.

The amount of rare-earth impurity in each experimental sample was determined by spectrographic analysis at a commercial laboratory to within 5% for the doping levels used. The error in impurity concentration affects only the absolute values of the intensities. Errors in determining the areas under the $k(\lambda)$ curves affect the relative intensities as well, and arise not only from instrumental errors in measuring a prescribed area, but also in determining the base line for zero rare-earth absorption when two or more transition groups lie close to one another. The instrumental error is

estimated to be 1% for the areas measured, although for a few extremely weak transitions this error may be as large as 25%. When the overlap area between two groups exceeded 5% of the total area for the two groups, the total area was measured and the matrix elements corresponding to the two transitions were combined and treated as a single experimental point in the fitting process.

IV. EXPERIMENTAL AND CALCULATED INTENSITIES

The observed transition intensities for $Pr^{3+}:Y_2O_3$, $Pr^{3+}:LaF_3$, $Nd^{3+}:Y_2O_3$, $Nd^{3+}:LaF_3$, $Eu^{3+}:Y_2O_3$, Er_2O_3, and Tm_2O_3 are presented in Tables I-VII. The corresponding calculated transition intensities are also listed in these tables, based on the sets of parameters for each system listed in Table VIII. Estimates of the statistical significance[15] of these parameters, reflecting the range of values a given parameter may take without seriously altering the rms deviation of the fitting, are also included in Table VIII. Discussion of the details of the fitting calculations for each system, matrix elements, number of levels used, etc., has been placed in an Appendix; the more pertinent discussion of the validity of the model and the interpretation of the resulting parameters follows immediately.

Table I. Measured and calculated f numbers for $Pr^{3+}:Y_2O_3$.

$[S',L']J'$	Energy, cm^{-1}	f number meas. (10^{-6})	f number calc. (10^{-6})	Δf (10^{-6})
$^3H_4$	2135		3.82	
$^3H_6$	4300	1.16	1.19	−0.03
$^3F_2$, $^3F_3$, $^3F_4$	5650	46.25	46.25	0.00
$^1G_4$	10 200	0.78	0.52	0.26
$^1D_2$	16 800	2.74	2.44	0.30
$^3P_0$, $^3P_1$, $^1I_6$, $^3P_2$	21 100	48.80	48.80	0.00
			rms dev. 9×10^{-6}	

Table II. Measured and calculated f numbers for $Pr^{3+}:LaF_3$.

S', L', J'	Energy, cm^{-1}	f number meas. (10^{-6})	f number calc. (10^{-6})	Δf (10^{-6})
$^3H_5$	2130	...	7.50	...
$^3H_6$	4277	...	0.63	...
$^3F_2$	5140	0.93	1.12	−0.19
$^3F_3$	6450	4.63	4.42	0.21
$^3F_4$	6859	2.96	3.22	−0.26
$^1G_4$	9800	0.10	0.08	0.02
$^1D_2$	16 835	0.97	0.76	0.21
$^3P_0$	20 750	0.94	1.07	−0.13
$^3P_1$, $^1I_6$	21 600	3.32	2.06	1.26
$^3P_2$	22 575	5.42	2.75	2.67
			rms dev. $= 1.34\times10^{-6}$	

Table III. Measured and calculated f numbers for $Nd^{3+}:Y_2O_3$.

$[S',L']J'$	Energy, cm^{-1}	*f* number meas. (10^{-6})	*f* number calc. (10^{-6})	Δf (10^{-6})
$^4I_{11/2}$	6250	0.13	0.15	−0.02
$^4F_{3/2}$	11 300	2.17	2.97	−0.80
$^4F_{5/2}$, $^2H_{9/2}$	12 315	6.78	6.82	−0.04
$^4F_{7/2}$, $^4S_{3/2}$	13 280	5.56	5.62	−0.06
$^4F_{9/2}$	14 490	0.65	0.49	0.16
$^2H_{11/2}$	16 050	0.14	0.14	0.00
$^2G_{7/2}$, $^4G_{5/2}$, $^2K_{13/2}$	16 950	41.64	41.73	−0.09
$^4G_{7/2}$, $^4G_{9/2}$	18 870	9.56	7.81	1.75
$^2G_{9/2}$, $^2K_{15/2}$, $^2D_{3/2}$, $^4G_{11/2}$	21 050	2.10	1.19	0.91
$^2P_{1/2}$, $^2D_{5/2}$	22 880	1.61	1.11	0.50
$^2P_{3/2}$	25 705	0.07	0.05	0.02
			rms dev. 0.78 (10^{-6})	

Table IV. Measured and calculated f numbers for $Nd^{3+}:LaF_3$.

$[S',L']J'$	Energy, cm^{-1}	*f* number meas. (10^{-6})	*f* number calc. (10^{-6})	Δf (10^{-6})
$^4I_{11/2}$	6130	0.11	0.11	0.00
$^4F_{3/2}$	11 590	1.09	1.44	−0.35
$^4F_{5/2}$, $^2H_{9/2}$	12 630	3.49	3.72	−0.23
$^4F_{7/2}$, $^4S_{3/2}$	13 600	3.79	3.67	0.12
$^4F_{9/2}$	14 830	0.32	0.27	0.05
$^2H_{11/2}$	16 050	0.06	0.08	−0.02
$^2G_{7/2}$, $^4G_{5/2}$, $^2K_{13/2}$	17 380	5.60	5.65	−0.05
$^4G_{7/2}$, $^4G_{9/2}$	19 440	3.50	2.46	1.04
$^2G_{9/2}$, $^2K_{15/2}$, $^2D_{3/2}$, $^4G_{11/2}$	21 510	0.86	0.44	0.42
$^2P_{1/2}$	23 470	0.22	0.37	−0.15
$^2D_{5/2}$	24 040	0.02	0.03	0.01
$^2P_{3/2}$	26 400	0.01	0.02	−0.01
			rms dev. 0.40 (10^{-6})	

Table V. Measured and calculated transition probabilities for $Eu^{3+}:Y_2O_3$.

S', L', J'	Energy, cm^{-1}	*A* meas., sec^{-1}	*A* calc., sec^{-1}	ΔA, sec^{-1}
$^7F_2$	12 215	···	20.	
$^7F_3$	13 215	0.0	0.0	0.0
$^7F_4$	14 285	75.0	75.0	0.0
$^7F_5$	15 270	24.1	0.0	24.1
$^7F_6$	16 310	732.3	732.3	0.0
$^7F_1$	16 860	98.0 *MD*	98.0 *MD*	0.0
$^7F_0$	17 190	6.2	0.0	6.2
	In absorption			
$^5D_0$	21 460	145.1	137.5	7.6
$^5D_1$	20 510	13.3 *MD*	13.3 *MD*	0.0
			rms dev. = 10.6 sec^{-1}	

Table VI. Measured and calculated f numbers for $Er^{3+}:Y_2O_3$.

S', L', J'	Energy, cm^{-1}	*f*-number meas. (10^{-6})	*f*-number calc. (10^{-6})	Δf (10^{-6})
$^4I_{13/2}$	6520	1.25	0.52 MD 0.73 ED	0.00
$^4I_{11/2}$	10 250	0.34	0.27	0.07
$^4I_{9/2}$	12 500	0.31	0.37	−0.06
$^4F_{9/2}$	15 210	1.73	1.44	0.29
$^4S_{3/2}$	18 200	0.34	0.24	0.10
$^2H_{11/2}$	19 180	11.03	9.95	1.08
$^4F_{7/2}$	20 360	1.13	1.34	−0.21
$^4F_{5/2}$, $^4F_{3/2}$	22 050	0.40	0.48	−0.04
$^2H_{9/2}$	24 500	0.61	0.67	−0.06
$^4G_{11/2}$	26 350	20.55	21.55	−1.00
$^2P_{3/2}$	31 210	0.03	0.07	−0.04
$^4G_{7/2}$	33 920	0.16	0.40	−0.24
$^2D_{3/2}$	34 600	0.09	0.07	0.02
$^4G_{5/2}$	36 350	0.57	1.22	−0.65
$^4D_{5/2}$, $^4D_{1/2}$	38 750	8.89	10.31	−1.42
			rms dev. = 0.50×10^{-6}	

Table VII. Measured and calculated f numbers for Tm_2O_3.

S', L', J'	Energy, cm^{-1}	f number meas. (10^{-6})	f number calc. (10^{-6})	Δf (10^{-6})
$^3H_6$	330	...	0.18[a]	...
$^3H_4$	5890	2.77	2.77	0.00
$^3H_5$	8340	2.66	0.60 MD 1.30 ED	0.76
$^3F_4$	12 690	2.96	2.97	−0.01
$^3F_3$	14 500	2.08	2.17	−0.09
$^3F_2$	15 180	0.39	0.37	0.02
$^1G_4$	21 500	1.13	1.14	−0.01
$^1D_2$	27 800	2.82	2.88	−0.06
$^3P_0$, $^1I_6$	34 750	3.32	1.46	1.86
$^3P_1$	36 000	1.95	0.72	1.23
$^3P_2$	37 900	4.72	4.34	0.38
$^1S_0$	82 000	...	0.04[a]	...

rms dev. = 0.91×10^{-6}

[a] This calculated f number does not include the index-of-refraction correction factor since the Cauchy dispersion fails in these spectral regions.

Table VIII. Experimental intensity parameters, $\bar{\Omega}_\lambda$.[a]

System	$\bar{\Omega}_2$ (10^{-20} cm^2)	$\bar{\Omega}_4$ (10^{-20} cm^2)	$\bar{\Omega}_6$ (10^{-20} cm^2)
$Pr^{3+}:Y_2O_3$	17.21±0.16	19.8 ±0.14	4.88±0.09
$Nd^{3+}:Y_2O_3$	8.55±0.43	5.25±0.80	2.89±0.61
$Eu^{3+}:Y_2O_3$	6.31	0.66	<0.48
$Er^{3+}:Y_2O_3$	4.59±0.25	1.21±0.21	0.48±0.33
$Tm^{3+}:Y_2O_3$	4.07±0.27	1.46±0.16	0.61±0.13
$Yb^{3+}:Y_2O_3$	3.5	1.75	0.80
$Pr^{3+}:LaF_3$	0.12±0.91	1.77±0.81	4.78±0.52
$Nd^{3+}:LaF_3$	0.35±0.14	2.57±0.36	2.50±0.33

[a] The values listed for $Yb^{3+}:Y_2O_3$ were determined by extrapolation of the experimental parameters of the other rare earths.

V. VALIDITY OF THE MODEL

The comparison of calculated and measured intensities, presented in Tables I-VII, shows that the simple phenomenological theory is able to account for all the salient features of the transition intensities of rare-earth ions in Y_2O_3 and LaF_3, and in several rare-earth oxides. The parameters found to describe each rare-earth system will depend somewhat on the method used to establish them, here the minimization of the sum of the squares of the deviations in line strengths. In this method, very weak transitions will play no role in determining the minimum condition, while very strong transitions will dominate in the selection of the minimizing parameters. This situation arises in the spectra of Nd^{3+} and Er^{3+} because of a number of very strong transitions, and yet the very weak transitions are reasonably well accounted for. The <u>average</u> rms deviation for all systems studied is 0.6×10^{-6} and the <u>average</u> observed f number for all systems is 4.8×10^{-6}. Thus, for the study as a whole the theory agrees with experiment to within about 12.5%. In addition to the measurement errors discussed previously, part of the discrepancy between theory and experiment can be attributed to failure of the experimental systems to completely meet the spectroscopic stability requirement for the validity of Eq. (3). The ground-state splittings of Pr^{3+}, Nd^{3+}, Er^{3+}, and Tm^{3+} in Y_2O_3 are 800, 560, 500, and 800 cm^{-1}, respectively. Thus the higher-lying Stark components of these J levels have considerably less population than the lower-lying Stark components at room temperature, this temperature being equivalent to an energy of about 210 cm^{-1}. However, because of the low crystal-field symmetry for Y_2O_3, each Stark component is represented by a linear combination of many different J_z basis states, and all possible values of J_z will appear in the wave functions of the Stark components occupied at room temperature. One might expect that the averaging over J_z states, producing Eq. (3), will in large measure still be met in Y_2O_3. Such large ground

J-level splittings in crystals of high symmetry might present more of a problem since certain values of J_z might not be occupied at room temperature, and these values of J_z may couple strongly to the excited f^n states.

Transitions involving more than a single phonon may contribute to the measured intensities, and this added intensity will not be accounted for by Eq. (3). While the matrix elements for these higher order processes are quite small, the density of states becomes large, and the process may not be completely negligible.

The experimental intensities for $Eu^{3+}:Y_2O_3$ exhibit some weak transitions, $^5D_0 \rightarrow {}^7F_0$, $^7F_3$, which violate selection[2] rules implicit in Eq. (3); similar violations have been observed in other systems.[16,17] These violations can most readily be explained by postulating the admixing of $J \neq 0$ into the $J = 0$ state via the crystal field, and/or the slight breakdown of the closure approximation[1] invoked to permit summing over excited configurations. This breakdown in closure would most be apt to happen in systems for which the 5d states lie close to the 4f states, as in Pr^{3+} and in divalent rare earths.

VI. INTERPRETATION OF EXPERIMENTAL PARAMETERS

The parameter sets for each rare-earth system in Y_2O_3 are plotted in Fig. 1 as a function of the number of 4f electrons. A logarithmic display is used to present the data because of the large range of values assumed by the parameters across the series. A smooth curve has been drawn through the experimental point to emphasize the trends across the series. The $\bar{\Omega}_2$ terms form a relatively slowly varying curve, while the curves formed by $\bar{\Omega}_4$ and $\bar{\Omega}_6$ show considerably more variation. These experimental parameters and their trends across the series can be used to investigate the validity of the use of free-ion excited-state radial wave functions in intensity calculations, and to determine what changes in these wave functions result from placing the free ion into the lattice. To this end, a calculation of the pertinent lattice sums is performed.

The Y_2O_3 host lattice forms in a cubic structure with two distinct types of cation sites, one with inversion symmetry of the point group C_{3i}, and the other with the relatively low symmetry of the point group C_2.[18] The unit cell contains three C_2 cation sites and a single C_{3i} cation site. It has been established[19] that rare-earth impurities enter both kinds of sites. Electric dipole transitions are of course forbidden for the ions in the C_{3i} sites, but their presence may contribute to the observed spectra by either vibronic or allowed magnetic dipole transitions.

The C_2 cation site[20] and its six nearest-neighbor oxygen ions is shown in Fig. 2. Four anions take up positions of near inversion symmetry with respect to the site origin, and therefore contribute to the odd-degree crystal-field expansion term only to the extent that inversion symmetry is distorted. The remaining anions have no inverted partners, and therefore account for the majority of the odd-degree crystal-field strength terms. The six nearest-neighbor anions take up positions described by the point group C_{2v}, which requires only half as many crystal-field terms as does the lower symmetry C_2 field. The nearest-neighbor cations are 12 Y^{3+}

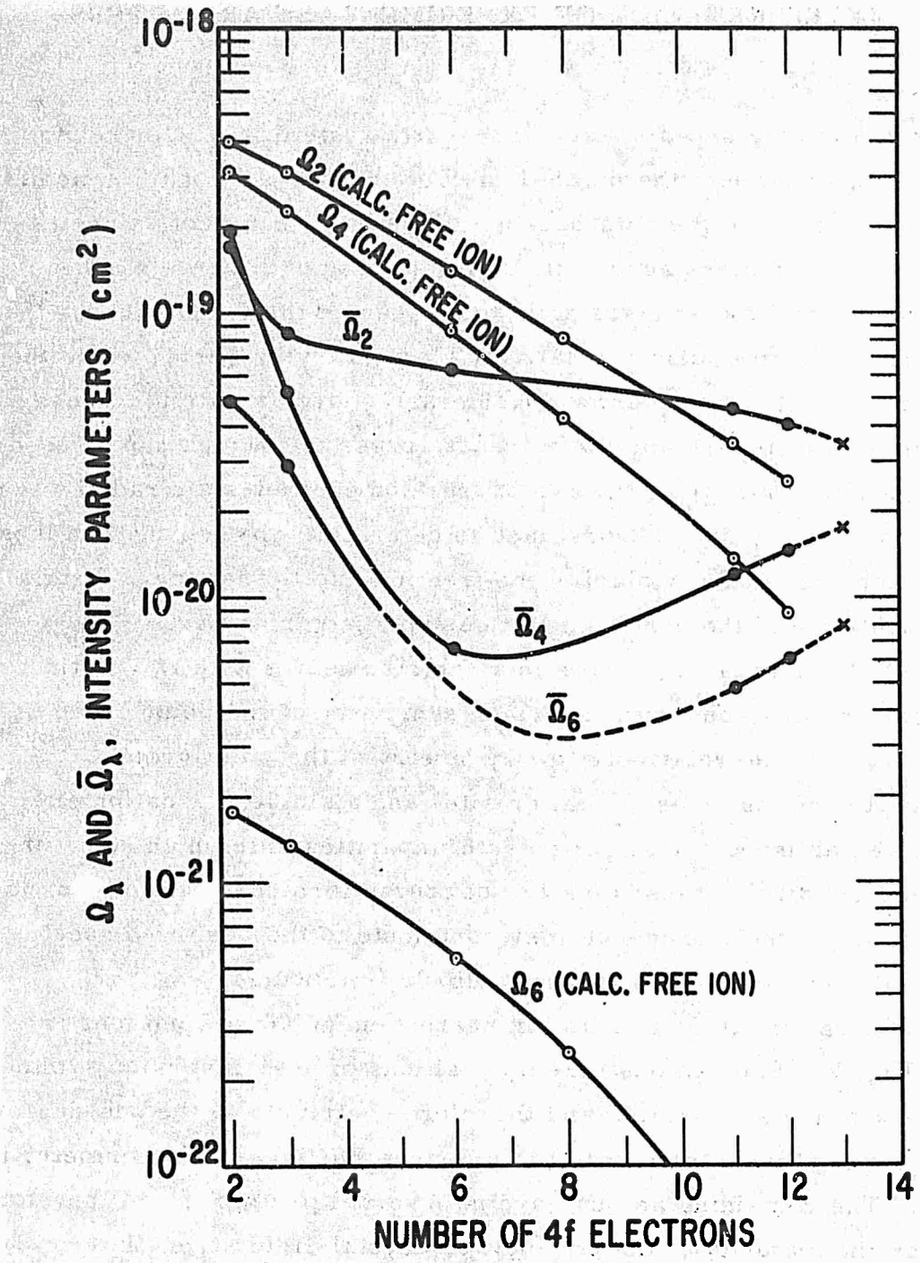

Fig. 1. Experimental intensity parameters ($\bar{\Omega}_\lambda$) and theoretical static intensity parameters (Ω_λ), based on free-ion radial wave functions as a function of the number of 4f electrons.

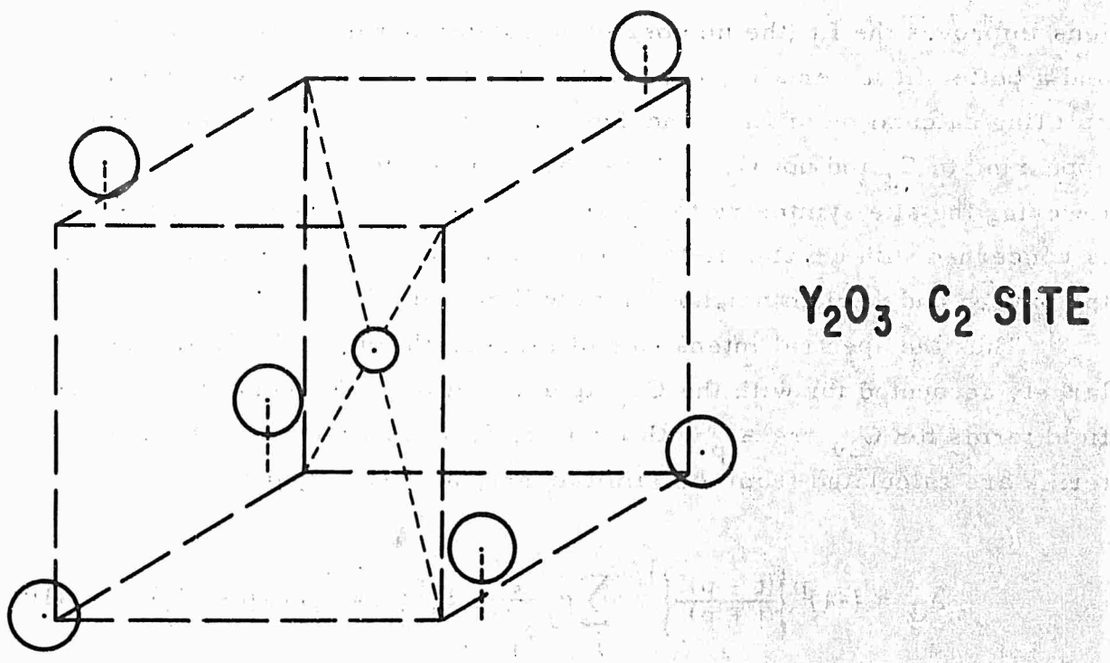

Fig. 2. Scale diagram of the C_2 cation site of Y_2O_3 showing the six nearest-neighbor oxygen ions. The cube center is located at the site origin; the cube diagonal is equal to twice the average distance of the six nearest neighbors. (This drawing was kindly provided by Dr. H. Tippins of this laboratory.)

ions which lie 1.67 times further away than the nearest-neighbor oxygen ions,[20] and which take up positions about the site origin with near inversion symmetry. These ions thus have virtually no effect on the intensities of rare-earth (RE) ions in the C_2 sites.[21] Finally, the 18 next-nearest oxygen ions lying 1.92 times further away than the nearest-neighbor oxygen ions, lower the site symmetry to C_2. Of these 18 ions, all but six are in positions of near inversion symmetry; the contribution of these six ions to the odd-degree terms of order t i s about $(1.92)^t$ times smaller than that of the nearest-neighbor oxygen ions. Moderate success has been achieved in fitting the crystal-field splitting of RE Stark levels in Y_2O_3 with the C_{2v}

approximation,[22] but inclusion of the effect of the next-nearest-neighbor ions improves the fit (the number of adjustable parameters doubles for C_2, and a better fit is certainly expected). The terms with $p < 0$ in the Stark-splitting calculation of Er^{3+} and Tm^{3+} in Y_2O_3 correspond to the terms appearing in C_2 and not C_{2v}. It can be seen that for the most part, terms lowering the site symmetry to C_2 are fairly small. Since the Stark splitting is concerned with crystal-field expansion parameters of even degree, all the oxygen and yttrium neighbor ions will be important.

Thus the spectral intensities of rare-earth ions in Y_2O_3 should be largely accounted for with the C_{2v} approximation. The nonzero odd crystal-field terms for C_{2v} are A_{tp} with t = 1, 3, 5, 7, and p even. The nonzero terms are calculated from the familiar crystal-field expansion

$$A_{tp} = (-1)^p \left\{ \frac{(t-p)!}{(t+p)!} \right\}^{1/2} \sum_j g_j \frac{e^2}{\rho_j^{t+1}} P_t^p(\cos \alpha_j) \exp(-ip\beta_j) \qquad (10)$$

where g_j ligand charges are located at the position $(\rho_j, \alpha_j, \beta_j)$ in spherical coordinates with respect to the rare-earth ion. The results of summing Eq. (10) over j for the six nearest-neighbor oxygen ions are listed in Table IX, along with the sums $\sum_p |A_{tp}|^2$, which will be required later.

Table IX. Odd-degree lattice sums for Y_2O_3, C_2 site.

p	A_{1p} (10^{-1} erg cm^{-1})	A_{3p} (10^{13} erg cm^{-3})	A_{5p} (10^{27} erg cm^{-5})	A_{7p} (10^{43} erg cm^{-7})
0	+2.25	−2.31	+2.15	+0.83
2	0	+1.57	+1.29	+1.46
4	0	0	+2.70	−4.90
6	0	0	0	+6.83

$$A_{10}^2 = 5.06 \times 10^{-8} \text{ erg}^2 \text{ cm}^{-2}$$
$$\sum_p |A_{3p}|^2 = 7.8 \times 10^{54} \text{ erg}^2 \text{ cm}^{-6}$$
$$\sum_p |A_{5p}|^2 = 1.36 \times 10^{55} \text{ erg}^2 \text{ cm}^{-10}$$
$$\sum_p |A_{7p}|^2 = 7.34 \times 10^{85} \text{ erg}^2 \text{ cm}^{-14}$$

Induced dipoles and higher order moments were not included in the lattice sum calculations above. Hutchings and Ray[23] have estimated the changes in the point-charge lattice sums of $LaCl_3$ due to these moments, with a 33% change in A_{20}, a 30% change in A_{40}, a 15% change in A_{60}, and a 1% change in A_{66}. The dipolar polarizability of oxygen is not too dissimilar from that of chlorine, and these values may be taken as fairly typical of the order of magnitude corrections to the lattice sums.

The expressions for $\Xi(t, \lambda)$ are[1]

$$\Xi(3,\lambda) = a(\lambda)\langle 4f|r|5d\rangle\langle 4f|r^3|5d\rangle/\Delta(5d) + b(\lambda)\sum_{n'}{}'\langle 4f|r|n'g\rangle\langle 4f|r^3|n'g\rangle/\Delta(n'g) \quad , \tag{11}$$

$$\Xi(5,\lambda) = c(\lambda)\langle 4f|r|5d\rangle\langle 4f|r^5|5d\rangle/\Delta(5d) + d(\lambda)\sum_{n'}\langle 4f|r|n'g\rangle\langle 4f|r^5|n'g\rangle/\Delta(n'g) \quad , \tag{12}$$

$$\Xi(7,6) = 28(\sqrt{55})/429 \times \sum_{n'}\langle 4f|r|n'g\rangle\langle 4f|r^7|n'g\rangle/\Delta(n'g) \tag{13}$$

with

$$a(2) = 8/35 \quad , \qquad b(2) = 4/7 \quad ,$$
$$a(4) = 2(\sqrt{22})/21 \quad , \qquad b(4) = 2(\sqrt{22})/77 \quad ,$$
$$c(4) = -20/33(\sqrt{70}) \quad , \qquad d(4) = -40/11(\sqrt{70}) \quad ,$$
$$c(6) = -10(\sqrt{14})/77 \quad ,$$

and

$$d(6) = -20/143(\sqrt{14}) \quad .$$

In these expressions, the expectation value of the radial coordinate and its powers are calculated between 4f and the excited 5d and n'g configurations. $\Delta(5d)$ and $\Delta(n'g)$ are the energy separations between the $4f^n$ ground configuration and the excited 5d and n'g configurations. The radial integrals between 4f and 5d states have been calculated for Pr^{3+} and Tm^{3+} free ions by Rajnak.[24] These values and the linearly interpolated values for the other rare-earth ions are listed in Table X. Dieke, et al,[25] have determined that the 5d states in the free ion lie about 50,000 cm^{-1} above the 4f configuration in Ce^{3+} and about 100,000 cm^{-1} above the 4f configuration in Yb^{3+}. These energy denominators and linearly interpolated values for the other ions are listed in Table X.

The required radial integrals have not yet been calculated for the n'g orbitals, and to proceed past this point, some approximation must be made. The completeness of the set of unoccupied n'g orbitals requires[1]

$$\sum_{n'} \langle 4f|r|n'g\rangle\langle 4f|r^t|n'g\rangle = \langle 4f|r^{t+1}|4f\rangle \qquad (14)$$

and the integrals on the right-hand side of Eq. (14) have been calculated for the free ions. To use Eq. (14) to simplify Eqs. (11), (12), and (13), the

Table X. Radial moments between 4f and excited electronic configurations, and energy denominators. All radial integrals are in atomic units; energy denominators are in units of 10^5 cm^{-1}.

	Pr^{3+}	Nd^{3+}	Eu^{3+}	Tb^{3+}	Er^{3+}	Tm^{3+}
$\langle 4f\|r\|5d\rangle$	0.90	0.87	0.78	0.71	0.62	0.58
$\langle 4f\|r^2\|5d\rangle$	5.47	5.17	4.26	3.66	2.75	2.45
$\langle 4f\|r^4\|5d\rangle$	50.5	47.1	36.9	30.1	19.9	16.5
$\langle 4f\|r^4\|4f\rangle$	5.34	4.96	3.83	3.08	1.95	1.57
$\langle 4f\|r^6\|4f\rangle$	39.6	36.4	26.5	20.1	10.5	7.3
$\langle 4f\|r^8\|4f\rangle$	500	450	320	232	100	62
$\Delta(5d)$	0.54	0.58	0.72	0.80	0.92	0.96
$\Delta(n'g)$	1.62	1.67	1.82	1.92	2.07	2.12

approximation must be made that the n'g configurations are closely spaced in energy compared to the energy separation of these configurations from the $4f^n$ configuration. This assumption is reasonably good for the bound g states which generally lie near the ionization limit. The rigorous validity of Eq. (14) requires the inclusion of the infinity of continuum orbitals with positive energy and large radial extension. The importance of the continuum states in the sum is not known. In fixing the value of the energy denominators for g-orbital contributions to the intensities, the ionization energy will be assumed with the understanding that this assumption will tend to maximize the calculated g-orbital contribution. Judd[1] has given arguments placing the energies of the bound n'g configurations of Nd^{3+} and Er^{3+} at 167,000 and 207,000 cm^{-1}, respectively. The corresponding values for the other rare-earth ions are listed in Table X.

The expansion for the static part of the intensity parameters is

$$\Omega_2 = (5/3)|A_{10}|^2\Xi^2(1,2) + (5/7)\sum_p |A_{3p}|^2\Xi^2(3,2) \quad , \qquad (15a)$$

$$\Omega_4 = (9/7)\sum_p |A_{3p}|^2\Xi^2(3,4) + (9/11)\sum_p |A_{5p}|^2\Xi^2(5,4) \quad , \qquad (15b)$$

$$\Omega_6 = (13/11)\sum_p |A_{5p}|^2\Xi^2(5,6) + (13/15)\sum_p |A_{7p}|^2\Xi^2(7,6) \quad . \qquad (15c)$$

In the process of calculating the theoretical Ω_λ parameters using free-ion radial wave functions, it is of considerable interest to keep track of the contributions from the d and g excited states. This has been done in Table XI, which presents the results of the calculation for the quantities $\Xi(t,\lambda)$. The calculated intensity parameters due to the static electric field are listed in Table XII. The contributions to the Ω_λ through the various crystal-field terms are listed individually in Table XII so that the most important crystal field terms can be readily identified. The theoretical

Table XI. Calculation of free-ion $\Xi(t, \lambda)$. All quantities associated with $\Xi(1, 2)$ are in units of 10^{-6} cm^{-2} erg^{-1}, with $\Xi(3, 2)$ and $\Xi(3, 4)$ in units of 10^{-22} cm^{4} erg^{-1}, with $\Xi(5, 4)$ and $\Xi(5, 6)$ in units of 10^{-38} cm^{6} erg^{-1}, and with $\Xi(7, 6)$ in units of 10^{-54} cm^{8} erg^{-1}.

Ion	$5d$	$n'g$	$\Xi(1,2)$	$5d$	$n'g$	$\Xi(3,2)$
Pr	−1.34	−0.44	−1.78	0.81	0.73	1.54
Nd	−1.17	−0.41	−1.58	0.69	0.66	1.35
Eu	−0.76	−0.32	−1.08	0.41	0.47	0.88
Tb	−0.56	−0.27	−0.83	0.28	0.36	0.64
Er	−0.37	−0.20	−0.57	0.16	0.20	0.36
Tm	−0.32	−0.18	−0.40	0.13	0.17	0.30
	$5d$	$n'g$	$\Xi(3,4)$	$5d$	$n'g$	$\Xi(5,4)$
Pr	1.60	0.15	1.75	−0.67	−1.59	−2.26
Nd	1.36	0.14	1.50	−0.56	−1.42	−1.98
Eu	0.80	0.10	0.90	−0.32	−0.95	−1.27
Tb	0.57	0.07	0.64	−0.21	−0.68	−0.89
Er	0.33	0.04	0.37	−0.11	−0.33	−0.44
Tm	0.26	0.03	0.29	−0.08	−0.22	−0.30
	$5d$	$n'g$	$\Xi(5,6)$		$n'g=\Xi(7,6)$	
Pr	−4.45	−1.00	−5.45		4.54	
Nd	−3.74	−0.89	−4.62		3.96	
Eu	−2.11	−0.59	−2.70		2.58	
Tb	−1.41	−0.43	−1.84		1.78	
Er	−0.71	−0.21	−0.92		0.71	
Tm	−0.52	−0.14	−0.66		0.43	

Table XII. Theoretical intensity parameters using free-ion radial wave functions. Ω_2 and Ω_4 are in units of 10^{-20} cm^2 and Ω_6 are in units of 10^{-21} cm^2.

Ion	A_{1p} terms	A_{3p} terms	Ω_2	A_{3p} terms	A_{5p} terms	Ω_4	A_{5p} terms	A_{7p} terms	Ω_6
Pr	26.74	13.24	39.98	30.68	0.57	31.25	0.48	1.31	1.78
Nd	20.91	10.16	31.07	22.44	0.44	22.88	0.34	1.00	1.34
Eu	9.70	4.26	13.96	8.12	0.18	8.30	0.12	0.43	0.54
Tb	5.79	2.35	8.14	4.16	0.09	4.25	0.05	0.20	0.25
Er	2.73	0.73	3.46	1.35	0.02	1.37	0.01	0.03	0.04
Tm	2.03	0.51	2.54	0.87	0.01	0.88	0.00$_7$	0.01	0.02

values for the Ω_λ parameters are plotted as a function of the number of 4f electrons in Fig. 1. In order to compare the theoretical static intensity parameters with the parameters found experimentally, the static contribution to the experimental parameters must first be established. Theory shows that the static intensity parameters decrease monotonically with increasing number of 4f electrons. Of the experimental curves, only $\bar{\Omega}_2$ has this form. The curves for $\bar{\Omega}_4$ and $\bar{\Omega}_6$ can be decomposed into two terms, one which varies across the series with a slope similar to that of $\bar{\Omega}_2$, and the other which increases as 4f electrons are either added to, or subtracted from, the half-filled 4f shell. The former term is associated with the static electric field contribution to intensities and the latter term with the vibronic contribution to the intensities. This decomposition of the experimental curves is consistent with the experimental fact that Pr and Tm ions exhibit intense vibronic structure in their spectra, Nd and Er ions exhibit distinctly less vibronic structure, and Eu ions exhibit virtually no vibronic structure. Thus in comparing theoretical and experimental parameter values for $\bar{\Omega}_4$ and $\bar{\Omega}_6$ only the values for Eu^{3+} may be used. There appears to be no tendency for the experimental $\bar{\Omega}_2$ curve to rise between Eu and Tm and it may be reasonably concluded that all of the experimental $\bar{\Omega}_2$ values arise predominantly from the static crystalline electric field, e.g., $\bar{\Omega}_2 = \Omega_2$.

The greatly differing slopes of the experimental and theoretical Ω_2 curves indicate at the outset a serious departure from the free-ion model in terms of which the radially dependent parts of Eqs. (15a)-(15c) were calculated. Because of the large range of values for the theoretical Ω_2 parameters, it is presumably coincidental that perfect agreement is obtained for ten 4f electrons. The calculated Ω_4 value for Eu is a factor of 12.5 larger than the experimental value, while the calculated Ω_6 value for Eu is a factor of 8.9 smaller than the experimental value (see Appendix). In accounting for the failure of the free-ion model to account for the intensity parameters, the effects of crystal-field shielding and distortion of radial wave functions must be considered.

A number of theoretical treatments of the linear[26-29] and nonlinear[30] shielding of 4f electrons from the electrostatic crystalline electric field resulting from distortion of the exterior $5s^2p^6$ closed shells by the lattice charges, have appeared in recent years. Numerical calculations have been most extensive for the rare-earth chlorides, and while estimates of the shielding of the A_{tp} for t even vary from calculation to calculation, it appears that substantial shielding does occur, being largest for t small. For example, Lenander and Wong[26] calculate a 59% shielding for A_{20}, 17% shielding for A_{40}. The shielding for A_{60} and A_{66} was not calculated but was estimated at less than 1%.

The failure of the electrostatic model to take into account the nephelauxetic[31] effect, or the expansion of the free-ion wave functions when the ion is embedded in a lattice, is of considerable importance also. This effect has been discussed[29] in connection with the inadequacy of the purely electrostatic model to account for the magnitude of the crystal-field Stark splitting of rare-earth levels in solids, and some useful estimates of the size of the effect were given. Quantitatively, the spherically symmetric core of the free ion is replaced by the core field produced by the ion and the field produced by the lattice charges. The core field will still be predominantly spherical but will possess lower symmetry components related to the lattice symmetry. The radial expansion of the wave functions will be accounted for by the spherically symmetric potential. Burns[29] estimates the quantity

$$\frac{\langle 4f|r^t|4f\rangle_{\text{lattice}} - \langle 4f|r^t|4f\rangle_{\text{free-ion}}}{\langle 4f|r^t|4f\rangle_{\text{free-ion}}}$$

to be 0.042, 0.12, and 0.36 for t = 2, 4, 6, respectively. By extrapolation the value is 1.08 for t = 8. Thus the expansion of the 4f radial wave function increases the radial moments r^t, being nearly negligible for t = 2 and doubling for t = 8. In the case of intensity calculations one would also like

to determine how the quantities $\langle 4f|r^t|5d\rangle$ behave in going from the free-ion to the ion in a lattice. The 4f radial wave function is always positive, while the 5d radial wave function has both positive and negative values. The 4f and 5d radial wave functions for Tm^{3+} calculated by Rajnak[24] were used to examine this question. The 5d function was expanded radially and renormalized, and the moments $\langle 4f|r^t|5d\rangle$ were numerically integrated. The moments for t equal to 3, 5, 7 were essentially unchanged from the free-ion values. The value of $\langle 4f|r|5d\rangle$, which is a common factor in all of the intensity parameters (see Eqs. 11 and 12), showed a marked decrease with radial expansion due to the relatively greater contribution of negative region of the 5d wave function. This integral is not positive definite, and if the expansion were severe enough, it could conceivably become negative.

From the discussion on shielding, it appears that the source of disagreement between calculated and measured Ω_6 parameters is not the shielding of the lattice sum value but the radial integral. A very similar disagreement occurs in the calculated and measured values of A_{t0} and A_{66} for the praeseodymium chloride lattice,[23] the calculated value being an order of magnitude too low. Remaining within the approximation Eq. (14), the increase in calculated Ω_6, which depends on $\langle 4f|r^8|4f\rangle$, by a factor of about 4 brings the calculated value in reasonably good agreement with the experimental value. The contribution to the parameters Ω_2 and Ω_4 from the $\ell = 4$ excited states are accounted for by the integrals $\langle 4f|r^2|4f\rangle$ and $\langle 4f|r^4|4f\rangle$ and are therefore essentially unaltered from the free-ion calculation.

The shielding of A_{10}, A_{3p}, and A_{5p} terms undoubtedly is partly responsible for the discrepancies in calculated and measured Ω_2 and Ω_4 parameters. Shielding would lower the calculated values as required by experiment. However, it is easy to see that shielding cannot account for all the discrepancy. The ratio of the experimental Ω_2 and Ω_4 parameters is $\Omega_2/\Omega_4 = 9.1$ for Eu^{3+} while the calculated ratio is only 1.7. Since greater shielding is expected in A_{10} than in A_{3p}, shielding would tend to make the calculated ratio smaller, in disagreement with experiment. The

calculated ratio can be brought into much better agreement with the experimental ratio by noting (see Tables XI and XII) that a reduction in the value of $\langle 4f|r|5d\rangle$ will greatly reduce the numerical values of Ω_4 while only slightly altering the numerical value of Ω_2. For instance, a factor of 5 reduction in the integral results in a new ratio $\Omega_2/\Omega_4 = 4.5$ and while this is still too low, it represents a considerable improvement. With this reduction of the importance of 5d contribution to intensities, the absolute value of the calculated Ω_4 term agrees quite well with the experimental values, 0.79×10^{-20} and 0.66×10^{-20} cm^2, respectively.

It is interesting to note that the intensity parameters calculated with the radial integrals modified for effects of the lattice, are composed predominantly of contributions from the $\ell = 4$ excited states; the percent g contributions are Ω_2(80%), Ω_4(50%), and Ω_6(100%). These results are consistent with the conclusion reached by Axe[3] for the spectrum of europium ethylsulfate. Parenthetically, this conclusion is of importance in estimating the electronic Raman cross sections for spontaneous and stimulated scattering by rare-earth ions in solids.[32] The expression for the cross section contains terms of the form $[\langle 4f|r|5d\rangle]^2$ and $\langle 4f|r^2|4f\rangle$. The former term will most likely be reduced an order of magnitude, based on the present work, while the latter term will be slightly increased when the ion is placed in a lattice. This serves to lower the Raman scattering cross sections by nearly an order of magnitude as compared with the cross sections calculated for the free ion.

Aside from the absolute values of the parameters, the problem of accounting for the greatly differing slopes of the Ω_2 curves remains. An analogous problem exists in explaining the slopes of the measured and calculated[29] even parity crystal-field terms for rare-earth ions in $LaCl_3$. Burns[29] has suggested that the source of this problem rests in a too simplified model for the lattice sum. By a detailed argument and supporting calculations, Burns suggests that the lattice charges are to be replaced by some effective charge located at the ionic radius of the rare-earth ion.

Because of the contraction of the ionic radius of rare earths with increasing number of 4f electrons amounting to a factor of about 1.2 across the series, each crystal-field lattice sum for Tm^{3+} will be larger than the corresponding term of Pr^{3+} by a factor of $(1.2)^{t+1}$ where t is the order of the term. This effect would result in a relative increase of Ω_2 for the Tm compared to that of Pr by a factor of 4.3, and would bring the slopes of the experimental and calculated Ω_2 curves into remarkably good agreement. A re-evaluation of the absolute values of the calculated curves would be necessary if such a model is assumed, and is beyond the scope of the present work.

In concluding the discussion of the experimental parameters, it can be observed that the vibronic interaction enters the $\bar{\Omega}_\lambda$ parameters via the elements $\partial A_{tp}/\partial Q_i$ from Eq. (6). Since the $\partial A_{3p}/\partial Q_i$ terms will be common to $\bar{\Omega}_2$ and $\bar{\Omega}_4$ and no vibronic interaction enters through the $\bar{\Omega}_2$ term, the elements $\partial A_{5p}/\partial Q_i$ must be significant for the Y_2O_3 lattice. It would be interesting to see if the direct calculation of these quantities bears this conclusion out, but the calculation would be quite extensive because of the large number of atoms in the unit cell.

VII. TRANSITION INTENSITIES IN RE:LaF_3

While the intensity data for the LaF_3 systems is not nearly so extensive, several interesting observations can be made. The Ω_2 parameters for Pr and Nd in LaF_3 are not statistically well defined, but it is clear that they are at least an order of magnitude smaller than the corresponding parameters for these ions in the Y_2O_3 lattice. The same comment is true for the Ω_6 parameters for both Pr and Nd are essentially identical for LaF_3 and Y_2O_3. These results imply that the value for the lattice sum A_{10} (with its shielding) is much smaller for the LaF_3 lattice (if it is formally allowed at all) than in the Y_2O_3 lattice. There is a classical argument that for lattice sites with point symmetries formally allowing an A_{10} term, its value will be identically zero, reflecting the fact that a finite electric field at the rare-earth nucleus is forbidden. As recently pointed out by Judd,[33] it is only the total electric field which must be zero at the rare-earth nucleus, and that distortions induced in the electron shells of the bound rare-earth ion produce an electric field at the nucleus opposing the lattice field. Moreover, Kiss and Weakliem[17] have recently found convincing experimental proof of the existence of a nonzero A_{10} lattice term. The experimental results of this study are also consistent with the existence of an A_{10} term.

In Judd's original[1] treatment of rare-earth intensities in solutions, it was observed that transitions for which $\Delta J = 2$ are peculiarly sensitive to changes in the ligands. Subsequently, Jorgensen and Judd[34] discussed the likely static and dynamic sources for this hypersensitivity. Noting that the J selection rule above for hypersensitive transitions is the condition for the matrix elements of $U^{(2)}$ to be nonzero, attention was focussed on mechanisms affecting Ω_2. Their calculations showed that the most likely mechanism is an asymmetrical distribution of the dipoles induced by the electromagnetic field in the medium. The gradient of the electric field across the rare-earth ion is greatly enhanced, resulting in greatly enhanced electric quadrupole transitions. Although not completely conclusive, a

recent experimental study of the hypersensitive transition $^5D_0 \rightarrow {}^7F_2$ of Eu^{3+} chelate[35] shows no evidence of the proposed "pseudoquadrupole" nature of the transition.

A comparison of the transition intensities for Nd^{3+} in Y_2O_3 and LaF_3 (Tables III, IV) shows that with the exception of the hypersensitive $^4G_{5/2}$ transition, the intensities in the Y_2O_3 lattice are a factor of 2 larger than in the LaF_3 lattice. Only the transition $^4I_{9/2} \rightarrow {}^4G_{5/2}$ possesses a significant $U^{(2)}$ matrix element. Instead of a relative increase by a factor of 2 for this transition in going from LaF_3 to Y_2O_3, a relative increase by a factor of 12 is observed. Since all the ions surrounding the rare-earth ions in these lattices have a uniform polarizability, no contribution from the pseudoquadrupole mechanism is possible for these systems, and yet a hypersensitive transition is observed.

In a re-evaluation of the sources of hypersensitivity in rare-earth spectra, Judd[33] suggests that the hypersensitivity arises from a simple change of point symmetry, the sensitive transitions being intense for point symmetries formally permitting an A_{10} term, and weaker for point symmetries formally excluding this term. The C_2 site symmetry permits an A_{10} term, as shown in the calculations above, and the hypersensitive $^4G_{5/2}$ is quite intense in Y_2O_3. The site symmetry for the rare-earth impurity in LaF_3 is still somewhat obscure. The structure of the LaF_3 lattice and the symmetry of the site of rare-earth impurities in this lattice have been studied by a number of techniques. Oftedal proposed[36] the structure of a hexamolecular unit cell with $D_{6h}{}^3$ symmetry. Subsequently, Schlyter[37] showed that all experimental evidence pointed to a bimolecular unit cell with $D_{6h}{}^4$ symmetry. The site symmetry for all metal ion sites is C_{2v} but not very far from D_{3h}. The paramagnetic resonance experiments of Jones, et al.,[38] and Baker and Rubins[39] confirm the C_{2v} site symmetry for rare-earth impurities. Optical studies on Nd^{3+}:LaF_3 by Wong, Stafsudd, and Johnson[40] showed evidence of selection rules not required by a C_{2v} site symmetry. Krupke and Gruber[41] also observed a partially polarized optical spectrum not predicted by a C_{2v}

symmetry. Finally, by studying the lattice vibrations of LaF_3, Caspers, Buchanan, and Marlin[42] conclude that room-temperature data should be accounted for by the bimolecular cell, with the metal ions in D_{3h} sites. They also point out that a small shift of approximately 0.05A is enough to change the crystal structure from the more symmetrical bimolecular cell to the hexamolecular cell. In the present study the D_{3h} point symmetry seems most appropriate since the intensity data was measured at room temperature. The A_{10} crystal-field expansion term is identically zero for this point symmetry. The relatively low intensity of the $^4G_{5/2}$ transition of Nd^{3+} in this point symmetry is thus expected, and experimentally supports the hypothesis that transition hypersensitivity arises from a simple change in point symmetry.

VIII. CONCLUSIONS

The generally good correlation between calculated and observed electric-dipole transition intensities for a number of rare-earth ions in a crystalline environment demonstrates the validity of the phenomenological aspects of the crystal-field-induced electric-dipole model. The determination of sets of phenomenological parameters for a number of different rare-earth ions in a common host lattice provides a profile of the parameters across the rare-earth series, against which the more fundamental aspects of the theoretical model were tested. The relative simplicity of the effective lattice charge distribution permitted a reasonably good estimate of the pertinent odd-degree crystal-field lattice parameters. While some inaccuracy in the lattice parameters is present, being based on a nearest-neighbor point-charge model, it has been shown that discrepancies occur between experimental parameters and those calculated using free-ion radial wave functions for the excited configurations, which cannot be attributed to the lattice calculation. It is concluded, semiquantitatively, that the $4f^{n-1}n'g$ configurations contribute somewhat more to the observed transition intensities than is indicated by the free-ion calculations, and that the $4f^{n-1}5d$ configuration contributes to the observed intensities about an order of magnitude less than indicated by free-ion calculations. Finally, the source of the hypersensitivity of the $^4I_{9/2} \rightarrow {}^4G_{5/2}$ transition of Nd^{3+} has been traced to a simple change in point symmetry about the ion for the two hosts.

APPENDIX

Rare-earth ions with a nearly filled 4f electron shell, such as erbium and thulium, form sesquioxides of the cubic structure with lattice parameters very nearly equal to those of Y_2O_3. Solid solutions of either Er_2O_3 or Tm_2O_3 with Y_2O_3 are possible in all mixtures. Rare-earth ions midway in the series, such as gadolinium with a half-filled shell, form sesquioxides with monoclinic structure, while rare-earth ions with nearly an empty 4f shell, such as neodymium and praseodymium, form sesquioxides with hexagonal structure. Only lightly doped Y_2O_3 crystals of Pr, Nd, and Eu were studied so as to remain within the cubic system. Y_2O_3 crystals lightly doped with Er and Tm were also studied, along with pure Er_2O_3, Tm_2O_3, and Yb_2O_3. The transition intensities of Pr and Nd trivalent ions in LaF_3 single crystals were studied for comparison with the results for the Y_2O_3 systems.

The matrix elements $\langle 4f^n[S,L]J||U^{(\lambda)}||4f^n[S',L']J'\rangle$ for each of the electronic configurations studied were calculated using intermediate coupling wave functions based on a free-ion fitting calculation of the observed levels of the rare-earth ion in Y_2O_3, when possible. The Racah and spin-orbit parameters for Y_2O_3 doped with thulium,[43] erbium,[44] and europium[45] have been reported, and those for Y_2O_3 doped with praeseodymium and neodymium[46] have been determined. A free-ion least-squares fitting of the published energy levels of praeseodymium[47,48] and neodymium[49] in LaF_3 produced Racah and spin-orbit parameters sufficiently similar to those found for the Y_2O_3 system that the intermediate coupling wave functions produced essentially identical intensity matrix elements. The sets of Racah and spin-orbit parameters used to calculate the $U^{(\lambda)}$ used in this study are set out in Table XIII. The value of the matrix elements calculated and used for this study agree with those reported subsequently by Carnall, et al.[5] The general insensitivity of the matrix elements for these ions in different host materials is due largely to the

Table XIII. Racah and spin-orbit parameters used to generate intermediate coupling wave functions

Ion	E^1, cm^{-1}	E^2, cm^{-1}	E^3, cm^{-1}	ζ, cm^{-1}
Pr^{3+}	4670.26	21.26	457.13	733.11
Nd^{3+}	4853.87	24.20	471.87	877.59
Eu^{3+}	6217.84	38.94	630.15	1343.1
Er^{3+}	6597.11	31.61	629.53	2383.0
Tm^{3+}	6722.19	33.88	663.45	2667.95

fact that the ground J levels are extremely pure, Pr^{3+} (98.7% triplet H), Nd^{3+} (98.4% quarter I), Er^{3+} (98.4% quartet I) and Tm^{3+} (99.5% triplet H). A direct comparison of the wave functions used here and those used by Carnall, et al.,[5] and by Axe[3] showed that even the excited state SL amplitudes of the intermediate-coupling wave functions varied only a few percent, and generally in weakly present SL components. In a few cases where the terminal excited state is predominantly of a different multiplicity than the ground state, several percent change was noted in the matrix elements. These transitions are usually weak and will therefore have little or no effect on the fitting parameters. For systems with highly mixed ground and excited states, the intensity matrix elements will be considerably more sensitive to the generating set of Racah and spin-orbit parameters (and possibly configuration interaction effects).

$Pr^{3+}:Y_2O_3$

The magnitude of the crystal-field Stark splitting of free-ion J levels is large in this host.[46] Because the spectrum of Pr^{3+} is fairly well compressed in energy, often Stark components of one J level cannot be easily distinguished from those of another J level. While one can obtain sufficient information about the energy centers of gravity from the low-temperature spectrum to attempt a free-ion energy-level calculation, the situation for interpreting room-temperature transition intensities is not so

simple. The components of the ^3P_J and $^1I_6$ J levels lie sufficiently close to one another that assignment of measured intensity components at 300°K to a specific J level is highly speculative. The same thing may be said about transitions terminating on components of the ^3F J levels. The total transition intensity measured in the vicinity of each of these two groups was treated as single experimental points. Transitions to three individual J levels could also be measured, producing a total of only five experimental points to be fit with three parameters. One would like to have more data to fit in order to more fully test the parameters, but it is of interest to obtain some estimate of the Pr^{3+} parameters for analysis of the whole series. The Pr concentration was spectrographically determined to be 1.56 at. %.

$Pr^{3+}:LaF_3$

The assignment of observed crystal-field levels to their parent J levels is considerably more reliable in LaF_3 than in Y_2O_3, primarily because of the smaller crystal-field splitting. One can resolve the intensities of transitions terminating on the $^3P_2$ and $^3P_0$ J levels while the total intensity for the combined $^1I_6$ and $^3P_1$ J levels is measured. Similarly, one can separate out the transition intensities for the $^3F_4$, $^3F_3$, and $^3F_2$ J levels with reasonable confidence. The rms deviation is rather large, 1.34×10^{-6}, and results primarily from the large deviation of the $^3P_2$ predicted and measured intensities. Since the predicted intensity for the $^3P_1 + {}^1I_6$ transition is also lower than measured, the explanation for the large discrepancy is not the overlap of crystal-field Stark components. J mixing by the crystal field for J levels so close in energy may be partially responsible, but similar discrepancies are not observed for similar transitions in other rare-earth systems. The significance of the resulting parameters is also doubtful, particularly the value of $\bar{\Omega}_2$, whose variance is larger than the absolute value. The absolute values of the parameters were determined by spectrographic analysis and the Pr doping found to be 0.7 at. %.

$Nd^{3+}:Y_2O_3$ and $Nd^{3+}:LaF_3$

A number of J levels of the $4f^3$ configurations lie close enough to another J level that their combined intensities must be used. Fortunately there are a sufficiently large number of separated levels for a good set of data to be used for fitting. The range in intensities of about 600 which is accounted for by this model demonstrates its basic validity. The absolute values for the parameters for both Y_2O_3 and LaF_3 were determined from the spectrographic analysis for the densities of Nd. The Y_2O_3 sample contained 1.36 at. % Nd and the LaF_3 sample contained 3.10 at. % Nd.

$Eu^{3+}:Y_2O_3$

Assignment of quantum numbers to most of the excited J levels of the Eu ion are at best tentative, and sufficient absorption data could not be obtained to determine the set of parameters $\bar{\Omega}_\lambda$. Because of the selection rule[2] that electric dipole transitions from a J = 0 level to a terminal J' level with J' odd are forbidden, there are only three allowed electric-dipole transitions between the metastable $^5D_0$ and the ^7F multiplet. The transition terminating on the $^7F_6$ proved to be too weak to detect in our experimental setup, so that a value for $\bar{\Omega}_6$ could not be determined for Eu. It can be inferred from the known minimum detectable power of the experimental system that $\bar{\Omega}_6$ must be less than 5×10^{-21} cm^2. The relative values of $\bar{\Omega}_2$ and $\bar{\Omega}_4$ were determined by the measured relative intensities of the fluorescence terminating on the $^7F_2$ and $^7F_4$ J levels, and no fitting was possible. The absolute parameter values were established by setting the measured magnetic-dipole intensity of the $^5D_0 \rightarrow {}^7F_1$ transition equal to the calculated magnetic-dipole intensity. This is equivalent to assuming a unit quantum efficiency for radiation when comparing calculated and measured electric-dipole transition rates, as in Table V. Although a fitting for Eu was not possible, a check on the absolute value of $\bar{\Omega}_2$ was

possible, by measuring in absorption the electric-dipole transition $^7F_0 \rightarrow {}^5D_2$, the components of the latter excited level being well established. The $\bar{\Omega}_2$ value determined from fluorescence predicted an f number of 5.3×10^{-7} and measured value was 5.6×10^{-7}. The Eu doping in the crystal of 5.15 at. % was determined from the measured and calculated magnetic-dipole absorption transition between the $^7F_0$ and $^5D_1$ J levels.

From the detailed analysis of the crystal-field Stark levels for $Eu^{3+}:Y_2O_3$ it is known[45] that all of the observed fluorescence transitions occur between electronic states alone, and no vibronic transitions are observed. This implies that the experimentally determined intensity parameters represent a purely static electric-field interaction.

$Er^{3+}:Y_2O_3$

This system provides an extensive test of the model since it was possible to fit 15 experimental intensities with only three parameters. Oscillator strengths as large as 2×10^{-5} and as small as 1×10^{-7}, a range of 200:1, were accounted for with an rms deviation of only 0.5×10^{-6}. The calculated magnetic oscillator strength for the $^4I_{15/2}$ to $^4I_{13/2}$ transition was subtracted from the measured intensity for this transition, and the remainder was assumed to be electric dipole in character. Measurements of transition intensities were made in pure Er_2O_3 samples and the relative intensities of transitions to various excited J levels were found to be independent of the doping. The absolute intensities of transitions were also found to be independent of the doping to within the accuracy of the spectrographic analysis of the doping in the dilute crystals. Thus the reported intensities and intensity parameters for Er_2O_3 are equivalent to those for $Er^{3+}:Y_2O_3$ for any concentration.

Tm_2O_3

The absorption intensities reported in Table VII were measured in pure Tm_2O_3, to avoid any uncertainty in Tm doping. The calculated oscillator strength of the magnetic-dipole transition $^3H_6 \rightarrow {}^3H_5$ was subtracted from the measured strength of this transition and the remainder was used in the fitting. As with the intensities in Er_2O_3 and $Er^{3+}:Y_2O_3$, the relative and absolute intensities for transitions measured in dilute $Tm^{3+}:Y_3O_3$ and in pure Tm_2O_3 were independent of Tm concentration to within the accuracy of the spectroscopic analysis for the Tm concentration in the dilute crystals.

Yb_2O_3

The spectrum of $Yb^{3+}:Y_2O_3$ or Yb_2O_3 consists of a single transition, $^2F_{7/2} \rightarrow {}^2F_{5/2}$ at an energy of about 10,000 cm^{-1}, and therefore an intensity fitting for three parameters cannot be made. The $U^{(\lambda)}$ for this one transition of Yb^{3+} are just the Russell-Saunders values, and the square of the expectation value is[5]

$$(1/196)[3\bar{\Omega}_2 + 10\bar{\Omega}_4 + 21\bar{\Omega}_6] \quad .$$

The $\bar{\Omega}_\lambda$ parameters established for the other rare-earth systems studied permit the extrapolation for the parameters expected for Yb^{3+}. Substitution of these values into the above expression yields an electric-dipole f number of 4.21×10^{-6}. The magnetic-dipole intensity is calculated to be 0.32×10^{-6}, for a total f number of 4.53×10^{-6}. The f number for this transition was measured to be 3.5×10^{-6} in a pure Yb_2O_3 sample. The 30% difference between calculated and measured intensities is somewhat larger than observed in the other rare-earth systems, but is not unacceptable considering the extrapolation that was involved.

REFERENCES

1. B. R. Judd, Phys. Rev. 127, 750 (1962).

2. G. S. Ofelt, J. Chem. Phys. 37, 511 (1962).

3. J. D. Axe, Jr., J. Chem. Phys. 39, 1154 (1963).

4. W. F. Krupke and J. B. Gruber, Phys. Rev. 139, A2008 (1965).

5. W. T. Carnall, P. R. Fields, and B. G. Wybourne, J. Chem. Phys. 42, 3797 (1965).

6. W. B. Fowler and D. L. Dexter, Phys. Rev. 128, 2154 (1962).

7. I. Richman, R. A. Satten, and E. Y. Wong, J. Chem. Phys. 39, 1833 (1963).

8. C. W. Nielsen and G. F. Koster, Spectroscopic Coefficients for p^n, d^n, f^n Configurations (MIT Press, Cambridge, Massachusetts, 1964).

9. M. Rotenberg, R. Bivens, N. Metropolis, and J. K. Wooten, The 3-j and 6-j Symbols (MIT Press, Cambridge, Massachusetts, 1964).

10. E. U. Condon and G. H. Shortley, The Theory of Atomic Spectra (Cambridge University Press, New York, 1957).

11. L. J. F. Broer, C. J. Gorter, and J. Hoogschagen, Physica 11, 231 (1945).

12. All crystal samples were grown by A. B. Chase, Aerospace Corporation.

13. K. A. Wickersheim and R. A. Lefever, J. Opt. Soc. Am. 51, 1147 (1961).

14. G. Haas, T. B. Ramsey, and R. Thun, J. Opt. Soc. Am. 49, 116 (1959).

15. E. B. Wilson, Jr., An Introduction to Scientific Research (McGraw-Hill Book Company, Inc., New York, 1952).

16. W. F. Krupke (unpublished).

17. Z. J. Kiss and H. A. Weakliem, Phys. Rev. Letters 15, 457 (1965).

18. L. Pauling and M. D. Shappell, Z. Krist. 75, 128 (1930).

19. M. Mandel, Appl. Phys. Letters 2, 197 (1963).

20. Ralph W. G. Wyckoff, Crystal Structures (Interscience Publishers, Inc., New York, 1963), Vol. 2.

21. It is for this reason that the electric dipole transition strengths for Tm^{3+} and Er^{3+} in Y_2O_3 and for Tm_2O_3 and Er_2O_3 are the same; that is, no distinction is made between the odd-symmetry field components produced by Y^{3+} and Er^{3+} at the site origin, since all terms cancel, while the oxygen ions which produce the observed intensities lie in very similar positions in these salts because of the close similarity of the lattice parameters. Moreover, the Y^{3+} ion has a closed 4p shell, and the Re^{3+} ion has a closed 5p shell, with ionic radii 0.92 and 0.89 Å, respectively. Thus from the outside, these ions appear quite similar, the principal difference being due to the radial wave function of the unfilled 4f shell of the Er or Tm. It is presumably this difference which gives rise to the quenching of fluorescence with increased Re doping, without altering the radiative interaction.

22. N. C. Chang (private communication). See also Ref. 43.

23. M. T. Hutchings and D. K. Ray, Proc. Phys. Soc. (London) 81, 663 (1963).

24. K. Rajnak, J. Chem. Phys. 37, 2440 (1962).

25. G. H. Dieke, H. M. Crosswhite, and B. Dunn, J. Opt. Soc. Am. 51, 820 (1961).

26. C. J. Lenander and E. Y. Wong, J. Chem. Phys. 38, 2750 (1963).

27. Gerald Burns, Phys. Rev. 128, 2121 (1962).

28. R. E. Watson and A. J. Freeman, Phys. Rev. 133, A1571 (1964).

29. Gerald Burns, J. Chem. Phys. 42, 377 (1965).

30. A. J. Freeman and R. E. Watson, Phys. Rev. 139, A1606 (1965).

31. C. K. Jorgensen, Orbitals in Atoms and Molecules (Academic Press, Inc., New York, 1962).

32. J. D. Axe, Jr., Phys. Rev. 136, A42 (1964).

33. B. R. Judd, J. Chem. Phys. 44, 839 (1966).

34. C. K. Jorgensen and B. R. Judd, Mol. Phys. 8, 281 (1964).

35. J. Blanc and D. L. Ross, J. Chem. Phys. 43, 1286 (1965).

36. Ivar Oftedal, Z. Physik. Chem. 6, 272 (1929); 13, 190 (1931).

37. K. Schlyter, Arkiv Kemi 5, 73 (1953).

38. D. A. Jones, J. M. Baker, and D. F. D. Pope, Proc. Phys. Soc. (London) 74, 249 (1959).

39. J. M. Baker and R. S. Rubins, Proc. Phys. Soc. (London) 78, 1353 (1961).

40. E. Y. Wong, O. M. Stafsudd, and D. R. Johnston, Phys. Rev. 131, 990 (1963).

41. W. F. Krupke and J. B. Gruber, J. Chem. Phys. 39, 1024 (1963).

42. H. H. Caspers, R. A. Buchanan, and H. R. Marlin, J. Chem. Phys. 41, 94 (1964).

43. J. B. Gruber, W. F. Krupke, and J. M. Poindexter, J. Chem. Phys. 41, 3363 (1964).

44. P. Kisliuk, W. F. Krupke, and J. B. Gruber, J. Chem. Phys. 40, 3606 (1964).

45. N C. Chang and J. B. Gruber, J. Chem. Phys. 41, 3227 (1964).

46. The author is indebted to Dr. N. C. Chang of this laboratory for communication of the detailed energy level data for $Nd^{3+}:Y_2O_3$ and $Pr^{3+}:Y_2O_3$ prior to publication.

47. E. Y. Wong, O. M. Stafsudd, and D. R. Johnston, J. Chem. Phys. 39, 1037 (1963).

48. W. M. Yen, W. C. Scott, and A. L. Schawlow, Phys. Rev. 136, A271 (1964).

49. E. Y. Wong, O. M. Stafsudd, and D. R. Johnston, Phys. Rev. 131, 990 (1963).

UNCLASSIFIED
Security Classification

DOCUMENT CONTROL DATA - R&D

(Security classification of title, body of abstract and indexing annotation must be entered when the overall report is classified)

1. ORIGINATING ACTIVITY *(Corporate author)*
Aerospace Corporation
El Segundo, California

2a. REPORT SECURITY CLASSIFICATION
Unclassified

2b. GROUP

3. REPORT TITLE
OPTICAL ABSORPTION AND FLUORESCENCE INTENSITIES IN SEVERAL RARE-EARTH-DOPED Y_2O_3 AND LaF_3 SINGLE CRYSTALS

4. DESCRIPTIVE NOTES *(Type of report and inclusive dates)*

5. AUTHOR(S) *(Last name, first name, initial)*
Krupke, William F.

6. REPORT DATE	7a. TOTAL NO. OF PAGES	7b. NO. OF REFS
June 1966	49	49

8a. CONTRACT OR GRANT NO.	9a. ORIGINATOR'S REPORT NUMBER(S)
AF 04(695)-669	TR-669(6230-25)-4
b. PROJECT NO.	
c.	9b. OTHER REPORT NO(S) *(Any other numbers that may be assigned this report)*
d.	SSD-TR-66-175

10. AVAILABILITY/LIMITATION NOTICES
This document is subject to special export controls, and each transmittal to foreign governments or foreign nationals may be made only with prior approval of SSD (SSTRT).

11. SUPPLEMENTARY NOTES	12. SPONSORING MILITARY ACTIVITY
	Space Systems Division Air Force Systems Command Los Angeles, California

13. ABSTRACT

The absolute intensities of transitions occurring in the optical spectra of single crystals of Y_2O_3 doped with small amounts of Pr, Nd, Eu, Er, and Tm; single crystals of LaF_3 doped with small amounts of Pr and Nd; and single crystals of Er_2O_3, Tm_2O_3, and Yb_2O_3 have been measured at room temperature. All observed transitions occur within the ground configurations of the trivalent rare-earth ions, and their intensities are accounted for using three phenomenological parameters for each system, whose values are determined by a least-squares fitting calculation. A calculation of the relevant crystal-field terms is made, and theoretical values for the intensity parameters are calculated using free-ion radial wave functions and certain closure approximations. It is concluded that excited $4f^{n-1}g$ configurations contribute to observed intensities more than is indicated by free-ion calculations, and that the excited $4f^{n-1}5d$ configuration contributes to the observed intensities an order of magnitude less than indicated by free-ion calculations. A hypersensitive transition in the neodymium systems is observed and its sensitivity is traced to a simple change in point symmetry of the host.

DD FORM 1473 (FACSIMILE)

UNCLASSIFIED
Security Classification

14.

KEY WORDS

Rare-Earth Spectra
Transition Intensities
Lasers
RE: Y_2O_3
RE: LaF_3

Abstract (Continued)